oceans

MDPI

Article

Impact of Indian Ocean Dipole Events on Phytoplankton Size Classes Distribution in the Arabian Sea

Rebekah Shunmugapandi *, Shirishkumar Gedam and Arun B. Inamdar

Center of Studies in Resources Engineering, Indian Institute of Technology Bombay, Mumbai 400076, India
* Correspondence: rebekah.s@iitb.ac.in

Abstract: Changes in the environmental condition associated with climatic events could potentially influence the PSC dynamics of the regional marine ecosystem. The Indian Ocean dipole (IOD) is one of the critical ocean–atmosphere interactions that affects the climate of the Arabian Sea, and it could be a potential factor influencing the regional PSC distribution. However, the relationship between PSC and IOD remains unclear and less explored. In this study, using the in-situ database acquired from the Arabian Sea, we reparametrized the three−component abundance−based phytoplankton size class model and applied it to reconstructed satellite−derived chlorophyll−*a* concentration to extract the fractional contribution of phytoplankton size classes to chlorophyll−*a* concentration. Further, we investigated the influence of IOD on the changes in the biological–physical properties in the Arabian Sea. The results showed that the biological–physical processes in the Arabian Sea are interlinked and the changes in the IOD mode control the physical variables like sea surface temperature (SST), sea surface height (SSH), and mixed layer depth (MLD), which influence the specific PSC abundance. Unprecedented changes in the PSC distribution and physical properties were observed during the extreme positive and negative IOD events, which clearly indicated the potential role of IOD in altering the PSC distribution in the Arabian Sea. This study highlights the impact of extreme climate events on PSC distribution and the need for a better understanding of the associated physical–biological–climate interactions.

Keywords: Arabian sea; phytoplankton size classes; physical forcing; IOD events; remote sensing

Citation: Shunmugapandi, R.; Gedam, S.; Inamdar, A.B. Impact of Indian Ocean Dipole Events on Phytoplankton Size Classes Distribution in the Arabian Sea. *Oceans* **2022**, *3*, 480–493. https://doi.org/10.3390/oceans3040032

Academic Editor: Antonio Bode

Received: 19 June 2022
Accepted: 10 October 2022
Published: 24 October 2022

1. Introduction

Phytoplankton, the basis of the oceanic food web, is an essential indicator of ocean ecosystem health [1,2]. In many studies, the phytoplankton biomass estimation is associated with the chlorophyll−*a* abundance (chl−*a*) (proxy of phytoplankton biomass), which is the primary, ubiquitous pigment commonly present in the phytoplankton [3–6]. However, oversimplifying phytoplankton as a single group does lead to a lack of detailed biological information about the phytoplankton groups and their unique environmental adaptation. The phytoplankton are diverse in nature and can be classified based on their taxonomy, size, and functional properties [7]. Each phytoplankton community is composed of a specific pigment composition that comprises a unique relationship with chl−*a* associated with a distinct taxonomic type and size through which the phytoplankton groups can be efficiently categorized [8–10]. Specifically, the size structure of phytoplankton has unique environmental adaptations and plays a significant role in the ocean's carbon cycle and marine food web [11]. The cell−size based classification of phytoplankton is widely categorized into micro (>20 µm), nano (2–20 µm), and pico (<2 µm) plankton [12].

Recent developments in abundance−based methods facilitated phytoplankton classification based on their size and functional traits from the total chl−*a* [13–18]. Each cell size has a unique pigment composition and a corresponding specific relationship with chl−*a*, from which the fractional contribution of each cell size to the total chl−*a* is retrieved [11,19]. In particular, the fraction of microplankton increases monotonically with the total chl−*a*,

and the fraction of nanoplankton shows a unimodal relation to the total chl−*a*. Likewise, the fraction of picoplankton decreases monotonically against the total chl−*a* [16,20–22]. The reparameterization of the existing abundance−based model based on the regional database will improve PSC detection for regional observations.

The continuous biological changes in the upper ocean can be observed through the advancements in satellite−derived data products, which provide the synoptic−scale measurements of chl−*a* [22–24]. The development of abundance−based phytoplankton community algorithms aided the retrieval of phytoplankton size classes (PSC) from the satellite retrieved ocean color observations (i.e., chl−*a* data products) [16,20]. Using a long−time series of biological information, many studies have explored the seasonal and spatial–temporal variability of PSC globally and regionally [15,25–27]. Beyond the seasonal and inter−annual responses, the PSC changes also facilitate the process, inferring their response to climatic events like El Niño Southern Oscillation (ENSO) and Indian Ocean Dipole (IOD) [28,29]. Many studies regarding the global ocean and regional basins have been carried out on the influence of IOD and ENSO phenomenon on phytoplankton as a single group [30–32]. However, the role of such climate events on the structure of the PSC is less explored.

The IOD is an anomalous ocean–atmosphere interaction like ENSO, which involves an irregular oscillation of sea–surface temperatures (SST) in the tropical Indian Ocean [33–35]. The IOD is defined by the difference in SST between the tropical western Indian Ocean and the tropical eastern Indian Ocean [32,36]. The strength of IOD is determined based on the Dipole Mode Index (DMI), which was developed by Saji et al. [36] to calculate the sea surface temperature anomaly (SSTA) difference between the tropical western Indian Ocean (50° E–70° E, 10° S–10° N) and tropical eastern Indian Ocean (90° E–110° E, 10° S–0° N) [36]. The DMI generally encounters two extreme conditions: (1) Positive DMI and (2) negative DMI. During positive DMI conditions, the strong southeasterly wind from the eastern Indian Ocean towards the western Indian Ocean causes warming (warmer SST) of the western Indian Ocean and cooling (colder SST) of the eastern Indian Ocean. In contrast, during negative DMI, the reverse conditions of the positive IOD occurs, therefore cooling (colder SST) the western Indian Ocean and warming (warmer SST) the eastern Indian Ocean [32,36,37]. Several studies have shown changes in chl−*a* concentration (phytoplankton biomass) influenced by the IOD in the Arabian Sea and the Indian Ocean. Brewin et al. [28] showed that, in the Indian Ocean, the phytoplankton community structure was influenced by the IOD and the relationship between the physical–biological interaction using a continuous 10−year time series of satellite observations. Thushara et al. [32] showed that, in the southeastern Arabian Sea, the unprecedented chl−*a* bloom occurred during the extreme nIOD event in 2016. Sharma et al. [38] observed the impact of strong pIOD events from 1997 to 1998 in the Arabian Sea, with a significant increase in SST and SSH leading to a corresponding decrease in chl−*a* distribution. As the PSC are sensitive to environmental drivers like SST, upwelling, and MLD, there are high chances of IOD influence on the PSC distribution. Therefore, it is essential to observe the impact of IOD on the PSC distribution in the regional seas of the Indian Ocean, which is less explored.

The Arabian Sea is among the sensitive and highly ecologically productive zones in the northern part of the tropical Indian Ocean [39–41]. Notably, the unique driving factor in the Arabian Sea region is the Indian monsoon, which plays an essential role in dictating the seasonal patterns of the phytoplankton community [42–44]. There is enough evidence that the IOD controls the physical drivers in the Arabian Sea [32,37]. Many studies revealed that the seasonal cycle in the Arabian Sea was often influenced by the IOD, which means that there is a high chance of IOD influencing the phytoplankton community structure [32,33,37,45]. However, limited studies have been conducted on the impact of IOD on biological changes, and the information on the IOD influence on the PSC assemblage is scarce. The investigation into the PSC response to strong positive and negative DMI provides a better opportunity to study the role of IOD on PSC distribution in the Arabian Sea.

The main objective of this study is to investigate the role of IOD on PSC distribution in the Arabian Sea. The main reason for carrying out this study was to understand the PSC sensitivity towards the changing DMI and the influence of IOD on the physical controls in the Arabian Sea. For this study, the regionally reparametrized three−component model found in Reference [13] was applied on 17−year gap−filled chl−*a* time−series data to extract PSC in the Arabian Sea. The derived datasets provide the synoptic−scale long−time series of the fractional contribution of each PSC to the total chl−*a*. Further, the DMI values were correlated with the PSC to identify the relationship between each PSC with DMI. Beside this, each PSC response to positive IOD and negative IOD events was then explored. Corresponding to the interannual variability of PSC, the sea surface temperature (SST), sea surface height (SSH), and mixed layer depth (MLD) products were used as the reference to identify the driving mechanism responsible for the PSC distribution in the Arabian Sea that corresponded to the IOD conditions.

2. Data and Methods

2.1. In Situ Database

The database of PSC and chl−*a* were gathered from field observations and various sources in the Arabian Sea. Both pigment and size−fractioned chl−*a* in situ datasets were used for this study. This includes the following datasets: Tara Ocean Expedition (TOE)−SEABASS database, SATCORE programme from ESSO−INCOIS, *Sagar Sampada* cruise (*SS2009*, *SS2010*, and *SS2011*), *Sagar Nidhi* cruise (*SN 128* and *SN137*), and Sagar Kanya cruise (*SN358*). The dataset information and sampling locations are shown in Figure 1 and Table 1. All the acquired PSC datasets are bound to the northern and eastern parts of the Arabian Sea due to the piracy issue along the western part of the Arabian Sea. As shown in Table 1, the PSC datasets were obtained from various sources. The datasets used in this study were composed of different measurement methods: HPLC, spectrophotometer, and fluorometer. The Tara Ocean Expedition (TOE) PSC datasets were obtained from the NASA SEABASS/NOMAD database, and the High−Performance Liquid Chromatography (HPLC) was used to extract phytoplankton pigment from the water samples. With the obtained pigment database, the PSC was measured using diagnostic pigment analysis (DPA) adapted from the work by [16] and [17]. For the Sagar Nidhi cruise, Sagar Sampada, and SATCORE database, the total chl−a and size−specific chl−*a* were collected using the filtration method. The total chl−*a* and size fractioned chl−*a* were calculated using a fluorometer for the samples from the Sagar Sampada cruise and a spectrophotometer for the SATCORE database and Sagar Nidhi cruise.

Table 1. Summary of the Arabian Sea cruises and in situ datasets.

SI NO	Cruise Information	Abbreviation	Location	Period	No of Samples
1	*Sagar Nidhi−128*	*SN*−128	Central Arabian Sea	January to February−2018	16
2	*Sagar Nidhi−137*	*SN*−137	Central Arabian Sea	January−2019	16
3	*Sagar Kanya−358*	*SK*−358	Central Arabian Sea	May−2019	16
4	*Sagar Sampada 2009*	*SS*−2009	Northern Arabian Sea	March−2009	8
5	*Sagar Sampada 2010*	*SS*−2010	Northern Arabian Sea	March−2010	3
6	*Sagar Sampada 2011*	*SS*−2011	Northern Arabian Sea	March−2011	17
7	*SATCORE−INCOIS*	SATCORE	Southern Arabian Sea	December−2013	95
8	*TARA Ocean Expedition*	TOE	Arabian Sea	March to April−2010	17

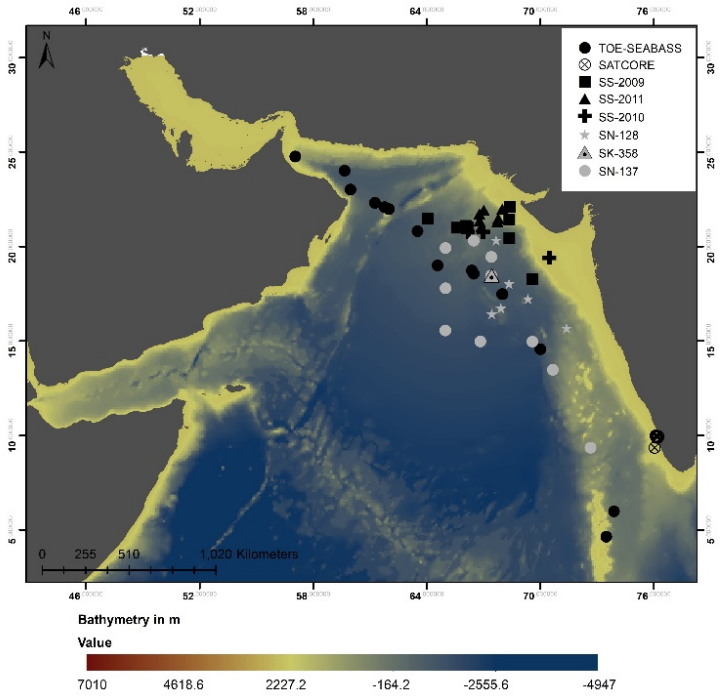

Figure 1. Map displaying the bathymetry of the Arabian Sea and the locations of the cruise sampling stations. Markers in grey represent the database obtained from field observations. Markers in black represent the database obtained from various sources.

Considering the total chl−*a* and PSC database obtained from different teams, the quality assurance processes were completed in the following way: Individual pigment and PSC data were visually checked, and the data of low quality (e.g., continuously repeated values, typically low values, values out of limit of measurement) were removed. Only surface samples were used to retune the three−component model, as this study intended to implement the model on satellite observations. Of 188 data points, 156 observations were scrutinized to reparametrize the model, from which ~10% (16) of datasets were retained for validation.

2.2. Model Reparameterization

In this study, the three−component model from Reference [13] was reparametrized based on the in situ PSC and total chl−*a* datasets obtained in the Arabian Sea and further applied to the satellite−observed chl−*a* to retrieve continuous PSC time−series. The in situ data collected from the Arabian Sea is the primary source for the model reparameterization. The nonlinear least square regression method was used to fit the 140 PSC in situ sample observation against the in situ chl−*a* to reparametrize the relationship between the PSC and the total chl−*a* derived from Reference [13]. The reparametrized three−component model estimates the size−specific chl−a (microplankton−C_m, nanoplankton−C_n, and picoplankton−C_p) to the total chl−*a*. In this model, the total chl−*a* is the sum of the C_m, $C_{n,}$ and C_p. The following was therefore obtained:

$$C = C_m + C_n + C_p \quad (1)$$

$$C_p = C_p{}^{max} [1 - \exp(-S_p\, C)] \quad (2)$$

$$C_{p,n} = C_{p,n}{}^{max} [1 - \exp(-S_{p,n}\, C)] \quad (3)$$

$$C_n = C_{p,n} - C_p \quad (4)$$

and

$$C_m = C - C_{p,n} \quad (5)$$

The total input chl−*a* is expressed as C [mg m^{-3}]; the subscripts m, n, and p refer to micro−, nano−, and pico plankton. The reparametrized $C_p{}^{max}$ = 0.253 and $C_{p,n}{}^{max}$ = 0.998, are the asymptotic maximum values of in situ C_p and $C_{p,n}$, respectively, and S_p is 2.692 and $S_{p,n}$ = 0.987, are the initial slope−corresponding relationship between C_p, $C_{p,n}$ and chl−*a*. The fraction of microplankton (F_m), nanoplankton (F_n), and picoplankton (F_p) to chl−*a* are obtained by dividing the C_m, C_n, and C_p by chl−*a*.

2.3. Satellite and Reanalysis Data

The present study is conducted based on a chl−*a* [mg m^{-3}] MODIS−Aqua Level−3 products, obtained from the NASA ocean color at daily and four−km resolution from the website (https://oceancolor.gsfc.nasa.gov/, accessed on 13 June 2020). The analyzed series covers the period from 2003 to 2019 for the Arabian Sea (43° E to 79° E and 0° N to 31° N). The satellite−based data products are generally prone to missing data values due to overcast conditions. The reconstruction of missing values is possible through the Data Interpolation Empirical Orthogonal Function (DINEOF), which was developed by the authors of Reference [46].

The DINEOF method is based on the Empirical Orthogonal Function (EOF), which reconstructs the missing data values with the number of EOF modes on an iterative basis. The DINEOF technique interpolates the missing values in the geophysical data using the singular vector decomposition (SVD) method. Initially, the time series datasets are transformed into the matrix, the values are demeaned, and the missing values are set to zero. Following this, 10% of the original chl−*a* satellite values were retained for cross−validation purposes. Subsequently, the input data matrix is decomposed through SVD iteratively with EOF modes until RMS converges. The same procedure continues with the number of EOFs modes until the optimum RMS converges. DINEOF is a freely available method that can be obtained from http://modb.oce.ulg.ac.be/mediawiki/index.php/DINEOF (accessed on 7 August 2019). Many studies have incorporated this method and successfully reconstructed oceanographic datasets like chl−*a* [3,26,47].

For comparison with physical variables other than SST, monthly−mean multi−mission observed sea surface height (SSH) data products and mixed layer depth (MLD) covering the period from 2003 to 2019 were acquired from the Copernicus Marine and Environment Monitoring Service (CMEMS) website (https://marine.copernicus.eu/, accessed on 8 July 2020). In addition, all the physical variables are spatially regridded corresponding to the PSC to efficiently compare the relationships on a pixel−by−pixel basis. The Indian Ocean Dipole Mode Index (DMI) data were downloaded from the NOAA ESRL Physical Sciences Laboratory website (https://psl.noaa.gov/gcos_wgsp/Timeseries/DMI/, accessed on 8 July 2020). The monthly PSC and physical properties anomalies were obtained from the 17−year climatology time series. Further, the changes in PSC and physical factors were investigated for the extreme positive (October 2019) and negative (July 2016) IOD events.

3. Results

3.1. Re−Parameterized Three−Component PSC Model

In this study, in situ phytoplankton measurements for the Arabian Sea from various sources and databases were used to reparametrize the three−component model to improve the retrieval of the regional−based size−specific chl−*a* in the Arabian Sea. Figure 2 shows the size−specific chl−*a* (C_{pn}, C_p, and C_m) relationship with the total chl−*a*. The reparametrized model efficiently estimates the relationship between the retrieved PSC and the total chl−*a* for the Arabian Sea (Figure 2). Figure 3 indicates the distinct relationship between each PSC and the chl−*a*. The fractional contribution of the microplankton (F_m) monotonically increases with the increasing chl−*a* (Figure 3a). The fractional contribution of nanoplankton (F_n) shows a unimodal relationship with the chl−*a*, whereas the fractional contribution of picoplankton (F_p) monotonically decreases with increasing chl−*a*. For the testing performance of the reparametrized model for the Arabian Sea, the similar PSC models from References [15,27,28] were compared using the mean absolute error

(MAE), Pearson correlation coefficient (r), and bias and root mean square error (RMSE) as evaluation metrics to compare in situ and model values. Table 2 shows the performance of the reparametrized PSC model for the Arabian Sea and similar PSC models using 10% of the datasets kept for validation (16 measurements).

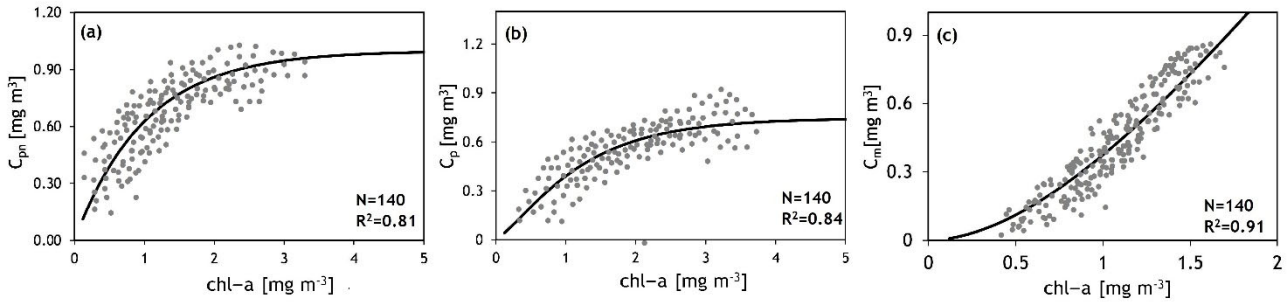

Figure 2. The in−situ size−specific chl−*a* plotted against the in situ chl−*a* [grey points]. (**a**) Pico + Nano plankton relation to total chl−*a*, (**b**) Picoplankton relation to total chl−*a*, and (**c**) microplankton in relation to total chl−*a*. The model fit is represented in a solid line.

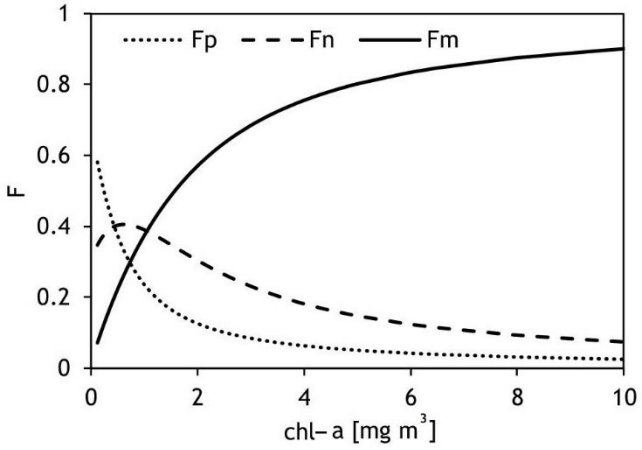

Figure 3. Regional relationship between in situ chl−*a* and model retrieved size fraction (F_m, F_n, and F_p).

Table 2. Statistical results of the validation.

	Pico			Nano			Micro			Region
	MAE	**BIAS**	**RMSE**	**MAE**	**BIAS**	**RMSE**	**MAE**	**BIAS**	**RMSE**	
This study	0.21	−0.11	0.21	0.12	0.07	0.16	0.12	0.04	0.12	Arabian Sea
Sahay et al. [27]	0.30	−0.28	0.35	0.18	0.08	0.20	0.17	0.10	0.19	Northern Arabian Sea
Brewin et al. [28]	0.31	−0.15	0.31	0.21	0.09	0.22	0.17	0.06	0.19	Indian Ocean
Hirata et al. [15]	0.27	−0.16	0.29	0.19	0.11	0.22	0.16	0.08	0.19	Global Ocean

Units in mg m^3.

3.2. Validation of Reconstructed Satellite Chl−a and PSC

To test the quality of the reconstructed chl−*a* for the appropriate input of the PSC model, we assessed it by comparing it with one−third of the in-situ database (i.e., 52) (Figure 4). From this evaluation, it was found that the efficacy of the DINEOF method was better at reconstructing the chl−*a*, which aided a gap−free chl−*a* as an input to perform the PSC model. Using the randomly selected (500 points) gap−filled satellite estimates of chl−*a* and fractional contribution of PSC (F_m, F_n, and F_p) obtained from the reparametrized three−component model, the relationships between the chl−*a* and F_m, F_n and F_p were observed to check whether the satellite estimates achieved the same relationship as in situ

PSC and chl−*a*, as shown in Figure 3. Figure 5a–c shows the relationship between the reconstructed satellite chl−*a* and satellite retrieved PSC from the reparametrized model for the Arabian Sea.

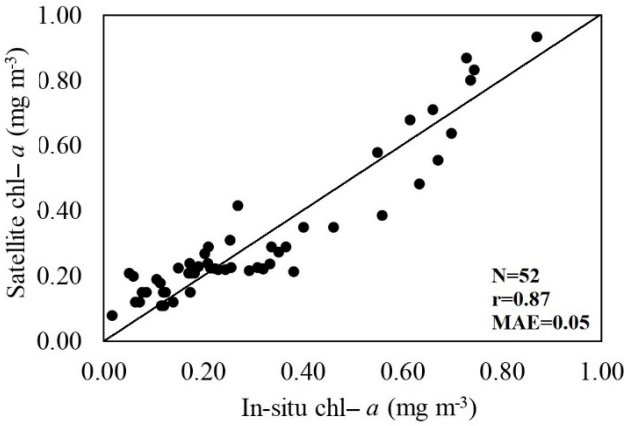

Figure 4. Validation of reconstructed satellite chl−*a* using the in situ chl−*a*.

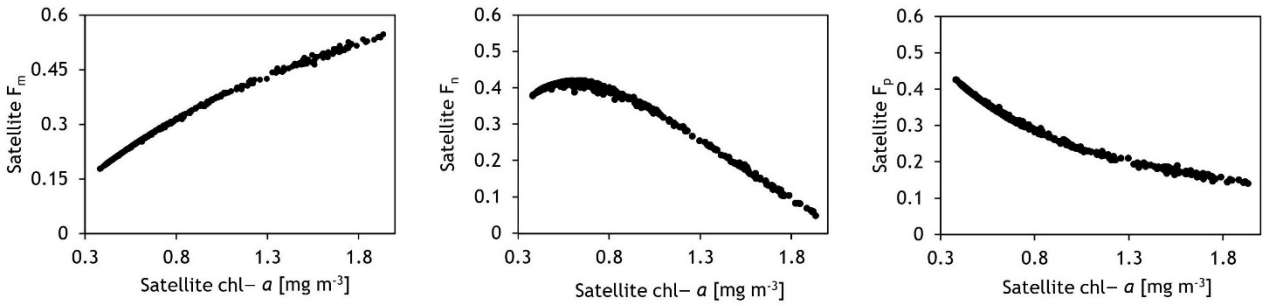

Figure 5. (**a–c**) shows the satellite−based PSC data extracted using a reparametrized three−component model plotted against the reconstructed satellite chl−*a*.

3.3. PSC and Physical Drivers vs. IOD

The continuous−time series of PSC anomaly datasets were computed by subtracting the PSC monthly time series from the PSC monthly climatology. Further, the PSC anomalies were assessed to examine the influence of IOD on the PSC distribution in the Arabian Sea, including the extreme and negative events of IOD indicated by the Dipole Mode Index (DMI). Figure 6 shows the monthly DMI for the period from 2003 to 2019 (17 years), where the positive value denotes the pIOD condition (positive IOD), and the negative value represents the nIOD condition (negative IOD). To understand the influence of DMI values on PSC distribution in the Arabian Sea, the DMI values were spatially correlated against the PSC anomalies over a 17−year time series. A significant correlation was observed between the specific PSC (micro and pico plankton) and the DMI in the Arabian Sea. Figure 7 shows the relationship between PSC, physical properties (SST, SSH, and MLD), and DMI. The correlation between the PSC versus DMI over the 17−year time series in the Arabian Sea indicates that a large distribution of negative correlation was observed between F_m and DMI.

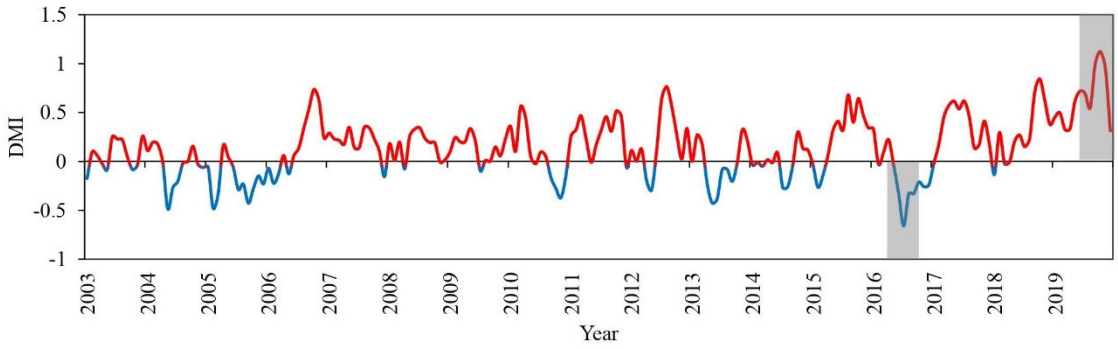

Figure 6. Temporal variation of the DMI for the period from 2003 to 2019, defined as the difference in SST anomalies between the western (50° E–70° E, 10° S–10° N) and eastern (90° E–110° E, 10° S–0° N) Indian Ocean [36]. The blue plot line represents negative IOD, and the red line represents positive IOD.

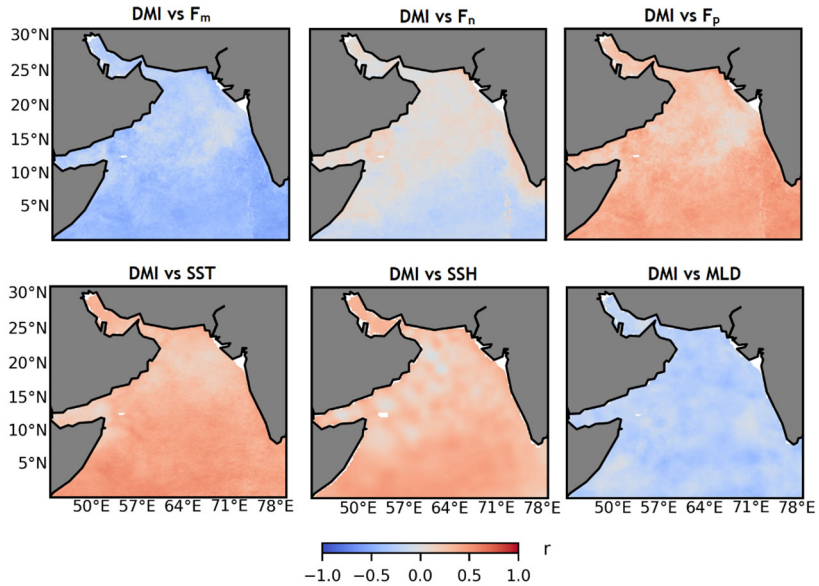

Figure 7. Correlation between the Indian Ocean–Dipole Mode Index and monthly anomalies of size fractioned chl−*a* (F_m, F_n, F_p), SST, SSH, and MLD. The correlations of DMI vs. PSC, SST, SSH, and MLD are statistically significant ($p < 0.05$).

On the contrary, a large distribution of positive correlation was observed between F_p and DMI. In comparison, no significant correlation was noticed between F_n and DMI in the Arabian Sea. Further, the DMI values were correlated against the physical variables to understand the SST and SSH response to DMI. The DMI versus physical variables shows a strong relationship, and a high distribution of positive correlation was observed between SST and SSH versus the DMI. In contrast, a high distribution of negative correlation was noticed between the MLD and DMI in the Arabian Sea.

To identify the influence of physical drivers on the PSC distribution, we further investigated the connection between the PSC and the physical variables like SST, MLD, and SSH in the Arabian Sea region, and the mean time−series anomalies of each PSC (F_m, F_n, and F_p) corresponding to the SST, MLD, and SSH was calculated. The biological and physical factors appeared to be closely correlated in the Arabian Sea. Figure 8 indicates that the inter−annual anomalies of F_p are largely positively correlated with the SST and SSH. This shows an inverse relationship with MLD, which coincided with the environmental adaptation of picoplankton. In contrast, the F_m showed a negative correlation with the SST and SST, and it had a positive relationship with MLD, which also coincided with favorable conditions for micro plankton. No correlation was observed between F_n and physical variables (SST, SSH, and MLD) as nanoplankton are ubiquitous. In Figure 8, the

microplankton, picoplankton and physical drivers appeared to be coupled throughout the Arabian Sea.

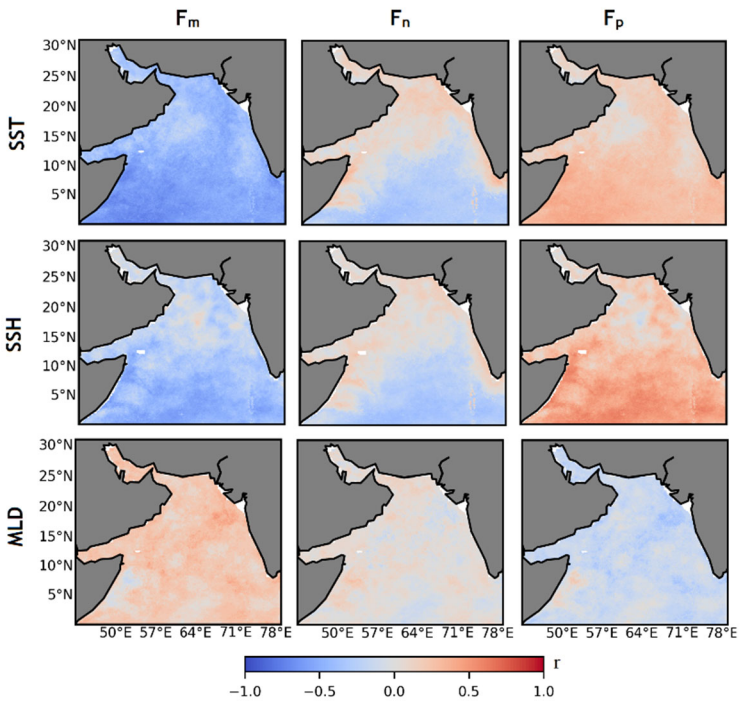

Figure 8. Relationship between physical drivers (SST, SSH, and MLD) and size fractioned chl−*a* (F_m, F_n, F_p). The correlation between the PSC (F_m, F_n, and F_p) and physical properties (SST, SSH, and MLD) are statistically significant ($p < 0.05$).

3.4. PSC and Physical Drivers Response to Extreme Positive and Negative IOD Events

The extreme negative (July 2016) and positive (October 2019) DMI periods were taken for the investigation to observe, in detail, how the extreme IOD climate events impact the PSC distribution in the Arabian Sea. Figures 9 and 10 shows the monthly anomaly maps of PSC and the physical variables (SST, SSH, and MLD) distribution in the Arabian Sea during the extreme nIOD and pIOD events. The changes in PSC and SST during the nIOD and pIOD periods were observed efficiently using the reconstructed chl−a input datasets. In July 2016 (nIOD), extreme positive anomalies were observed in SST and SSH over the Arabian Sea (Figure 9). A large corresponding distribution of positive anomalies was observed in F_m. In contrast, a wide distribution of negative anomalies was observed in F_p. When the F_n anomalies were noticed, it was understood that the extreme nIOD event did not show any significant connection with the F_n assemblage. In December 2019 (pIOD), extreme negative anomalies were observed in SST and SSH (Figure 10). A large distribution of negative anomalies was observed in F_m. On the contrary, an extensive distribution of positive anomalies was observed in F_p anomalies. No significant changes were observed in the Arabian Sea on the F_n anomalies.

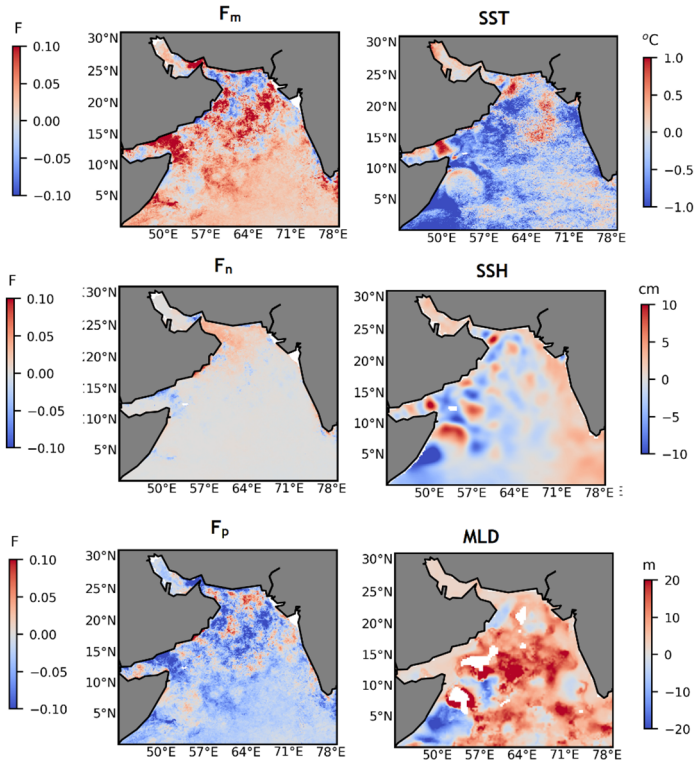

Figure 9. Monthly anomaly map of F_m, F_n, F_p, SST, SSH and MLD during the extreme negative IOD (July 2016) in the Arabian Sea.

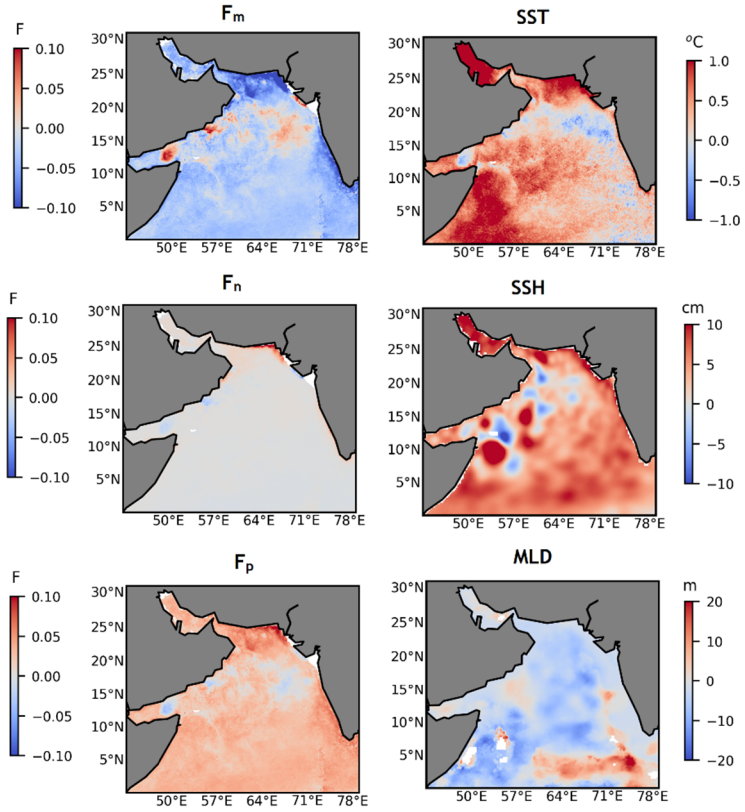

Figure 10. Monthly anomaly F_m, F_n, F_p, SST, SSH and MLD during the extreme positive IOD (October 2019) in the Arabian Sea.

4. Discussion

The Indian monsoon and the IOD are the primary drivers controlling physical and biological interactions in the Arabian Sea. As the phytoplankton communities are sensitive by nature and have a unique favorable condition, fluctuations in the IOD can highly impact the phytoplankton distribution. The present study investigated the unique relationship between each PSC and IOD in the Arabian Sea using the reparametrized PSC model. Several studies have shown changes in chlorophyll−a concentration (phytoplankton biomass) influenced by the IOD in the Arabian Sea and the Indian Ocean. Brewin et al. [28] showed that, in the Indian Ocean, the phytoplankton community structure was influenced by the IOD and the relationship between the physical–biological interaction using a continuous 10−year time series of satellite observations. Thushra et al. [32] showed that, in the southeastern Arabian Sea, the unprecedented chl−*a* bloom occurred during the extreme nIOD event in 2016. Sarma et al. [38] showed the impact of strong pIOD events during 1997–1998 in the Arabian Sea with a significant increase in SST and SSH, which led to a corresponding decrease in chl−*a* distribution.

Our study investigated the relationship between each PSC and the DMI conditions, highlighting the importance of the regional phytoplankton community−wise responses to climate events. Even though the significant influence of IOD on the physical dynamics and its impact on the chl−*a* distribution in the Arabian Sea have been well documented, the PSC responses are less explored, so we attempted to investigate this in this study. Satellite−derived PSC obtained using the regionally reparametrized PSC model were closer to the PSC in situ values compared to other similar models for the Arabian Sea. The specific constraint on using the satellite datasets was the missing data values due to cloud conditions that were resolved using the gap−filling method (DINEOF) by reconstructing the missing data values. The gap−filled 17−year continuous chl−*a* enhanced the spatial coverage of PSC distribution, which facilitated further investigation of the unique relationship between each PSC, physical variables, and IOD in the Arabian Sea.

The observed correlations between the PSC, physical variables, and DMI show the distinct responses of each PSC to the changing environmental conditions. The changes in physical drivers, such as SST, SSH, and MLD corresponding to IOD, showed the influence of IOD on the physical processes and the impact on PSC distribution. The results showed evidence that the physical, biological and chemical processes in the Arabian Sea are interlinked (Figures 7 and 8). Our study examined the fundamental theories of biological−physical processes and ecosystem structures. The microplankton tendency to dominate in mixed waters and under high nutrient conditions is related to colder SST, low SSH, and deeper MLD [11,15,19,48]. The picoplankton prefers to live in a stratified and oligotrophic environment associated with warmer SST, high SSH, and shallow MLD [11,19,48]. In contrast, nanoplankton is ubiquitous and capable of surviving in any conditions [11,19,48].

In the Arabian Sea, the summer and winter monsoon are responsible for the changing physical processes and corresponding seasonal distribution of PSC, which have been discussed in detail in Reference [26]. During the summer monsoon period (June–September), the summer upwelling process in the southwestern part of the Arabian Sea (near the Oman coast) creates optimal conditions for the microplankton to dominate in the specific location. In Figure 9, the extreme nIOD anomaly map showed the widespread positive microplankton anomaly, negative picoplankton anomaly, and associated physical conditions throughout the Arabian Sea, which is an unprecedented change that occurred due to the impact of extreme nIOD. In October, the offset of the summer monsoon leads to the decline of microplankton abundance. In Figure 10, the extreme pIOD anomaly map showed an unusual positive anomaly of picoplankton throughout the Arabian Sea, especially in the north part of the Arabian Sea, which has not been reported elsewhere because picoplankton usually dominates in the southernmost part of the Arabian Sea due to its oligotrophic behavior. The impact of extreme pIOD could be the reason for the unprecedented changes in the distribution of PSC in the Arabian Sea. Nanoplankton anomaly maps indicated the ubiquitous behavior of nanoplankton towards the extreme nIOD and pIOD events. From

the observation of the instance of extreme IOD events, it is understood that extreme IOD events influenced the physical drivers, led to changes in the physical properties in the Arabian Sea and impacted the PSC structure.

The present study emphasizes that climatic drivers, such as IOD interaction, influences the physical–biological dynamics of the Arabian Sea. This study showed that each PSC has a distinct response to the IOD, which could likely facilitate a definite ecological province and the structure of the biogeochemical cycles in the Arabian Sea. Our approach is restricted to the size−based classification of phytoplankton, which is the first−order approximation of chlorophyll−*a*. Developing a method to study phytoplankton species may provide a better understanding of how the phytoplankton species in the regional ecosystem respond to the changing climate.

5. Conclusions

The present study reparametrized the three−component model for the Arabian Sea, which was applied on a 17−year time series of gap−filled chl−*a* observations of MODIS−Aqua satellite data from 2003 to 2019 to retrieve PSC continuous datasets. The gap−filled spatial coverage of the chl−*a* time series was achieved using the DINEOF approach. The continuous spatial and temporal fields of PSC for 17−years were efficiently obtained through this approach.

A novel contribution of this study is the capacity to explore the PSC response to the IOD events and physical processes to get a better understanding of the factors controlling the PSC distribution. The results of the observation of the relationship within DMI, microplankton, picoplankton, SST, SSH, and MLD showed that the changes in the distribution of micro and picoplankton are associated with the physical drivers controlled by the IOD. The present study explored the extreme IOD events' impact on the PSC distributions and observed the unprecedented changes in the biological and physical processes. Thus, the overall study delineates the characteristics of PSC and their response to the changing environmental condition influenced by the IOD in the Arabian Sea. Our findings encourage further studies on phytoplankton community responses to regional and global climatic events.

Author Contributions: Conceptualization, R.S., S.G. and A.B.I.; methodology, R.S. and S.G.; software, R.S. and S.G.; validation, R.S., S.G. and A.B.I.; formal analysis, R.S.; investigation, R.S.; resources, R.S., S.G. and A.B.I.; data curation, R.S. and S.G.; writing—original draft preparation, R.S.; writing—review and editing, R.S., S.G. and A.B.I.; visualization, R.S.; supervision, S.G. and A.B.I.; project administration, S.G.; funding acquisition, R.S. and S.G. All authors have read and agreed to the published version of the manuscript.

Funding: This research was funded by INSPIRE Department of Science and Technology grant number IF170191.

Institutional Review Board Statement: Not applicable.

Informed Consent Statement: Not applicable.

Data Availability Statement: The data presented in this study are available on request from the corresponding author.

Acknowledgments: The authors thank NASA's Ocean Biology Processing Group (OBPG) for the open−source chl−*a* concentration and SST data and CMEMS for the SSH and MLD datasets. The authors thank all contributors to the NASA SeaBASS/NOMAD database for in situ pigment data. We greatly acknowledge the support from Aneesh Lotliker, Girishkumar M.S, and Sanjiba kumar baliarsingh, ESSO−INCOIS for helping in in situ measurements and analysis. The authors thank the ESSO−INCOIS and NCPOR (Ministry of Earth Sciences, MoES), the NIOT (MoES) for the expedition facility, and the crew for onboard cooperation. Srinivas Kolluru, Chandanlal Parida, Madhusmitha Das, and Sudatta Prathiba are acknowledged for their assistance during in situ collection and analysis. We are grateful to Director, ESSO−INCOIS and SATCORE team for providing an in situ database through the SATCORE programme. The authors express special gratitude to Jocquim Goes, Lamont−Doherty Earth Observatory (LDEO), for supporting this study by providing *Sagar Sampada* (2009, 2010, 2011) in situ datasets. We thank the Department of Science and Technology for supporting this research through the DST−INSPIRE fellowship programme [Grant no: IF170191].

Conflicts of Interest: The authors declare no conflict of interest.

References

1. Legendre, L.; Le Fèvre, J. From Individual Plankton Cells To Pelagic Marine Ecosystems And To Global Biogeochemical Cycles. In *Particle Analysis in Oceanography*; Demers, S., Ed.; Springer: Berlin/Heidelberg, Germany, 1991; pp. 261–300. ISBN 978-3-642-75121-9.
2. Brody, S.R.; Lozier, M.S.; Dunne, J.P. A Comparison of Methods to Determine Phytoplankton Bloom Initiation. *J. Geophys. Res. Ocean* **2013**, *118*, 2345–2357. [CrossRef]
3. Andreo, V.C.; Dogliotti, A.I.; Tauro, C.B. Remote Sensing of Phytoplankton Blooms in the Continental Shelf and Shelf−Break of Argentina: Spatio−Temporal Changes and Phenology. *IEEE J. Sel. Top. Appl. Earth Obs. Remote Sens.* **2016**, *9*, 5315–5324. [CrossRef]
4. Mangesh, G.; Siby, K.; Damodar, S.M.; Hema, N.; Naqvi, S.W.A. Cyclone Phyan−Induced Plankton Community Succession in the Coastal Waters off Goa, India. *Curr. Sci.* **2016**, *111*, 1091–1097. [CrossRef]
5. Raghavan, B.R.; Raman, M.; Chauhan, P.; Sunil Kumar, B.; Shylini, S.K.; Mahendra, R.S.; Nayak, S.R. Summer Chlorophyll−a Distribution in Eastern Arabian Sea off Karnataka−Goa Coast from Satellite and in−Situ Observations. *Remote Sens. Mar. Environ.* **2006**, *6406*, 64060W. [CrossRef]
6. Winder, M.; Cloern, J.E. The Annual Cycles of Phytoplankton Biomass. *Philos. Trans. R. Soc. B Biol. Sci.* **2010**, *365*, 3215–3226. [CrossRef]
7. Kostadinov, T.S.; Cabré, A.; Vedantham, H.; Marinov, I.; Bracher, A.; Brewin, R.J.W.; Bricaud, A.; Hirata, T.; Hirawake, T.; Hardman−Mountford, N.J.; et al. Inter−Comparison of Phytoplankton Functional Type Phenology Metrics Derived from Ocean Color Algorithms and Earth System Models. *Remote Sens. Environ.* **2017**, *190*, 162–177. [CrossRef]
8. Bricaud, A.; Babin, M.; Morel, A.; Claustre, H. Variability in the Chlorophyll−Specific Absorption Coefficients of Natural Phytoplankton: Analysis and Parameterization Phytoplankton a • h (A) Was Analyzed Using a Data Set Including 815 Spectra Determined Chlorophyll Concentration Range Ph Values Wer. *J. Geophys. Res.* **1995**, *100*, 13321–13332. [CrossRef]
9. Ciotti, A.M.; Bricaud, A. Retrievals of a Size Parameter for Phytoplankton and Spectral Light Absorption by Colored Detrital Matter from Water−Leaving Radiances at SeaWiFS Channels in a Continental Shelf Region off Brazil. *Limnol. Oceanogr. Methods* **2006**, *4*, 237–253. [CrossRef]
10. Kheireddine, M.; Ouhssain, M.; Organelli, E.; Bricaud, A.; Jones, B.H. Light Absorption by Suspended Particles in the Red Sea: Effect of Phytoplankton Community Size Structure and Pigment Composition. *J. Geophys. Res. Ocean.* **2018**, *123*, 902–921. [CrossRef]
11. IOCCG. *Phytoplankton Functional Types from Space*; Reports and Monographs of the International Ocean Colour Coordinating Group; International Ocean−Colour Coordinating Group: Dartmouth, NS, Canada, 2014; p. 156.
12. Sieburth, J.M.N.; Smetacek, V.; Lenz, J. Pelagic Ecosystem Structure: Heterotrophic Compartments of the Plankton and Their Relationship to Plankton Size Fractions. *Limnol. Oceanogr.* **1978**, *23*, 1256–1263. [CrossRef]
13. Brewin, R.J.W.; Sathyendranath, S.; Hirata, T.; Lavender, S.J.; Barciela, R.M.; Hardman−Mountford, N.J. A Three−Component Model of Phytoplankton Size Class for the Atlantic Ocean. *Ecol. Model.* **2010**, *221*, 1472–1483. [CrossRef]
14. Brewin, R.J.W.; Raitsos, D.E.; Dall'Olmo, G.; Zarokanellos, N.; Jackson, T.; Racault, M.F.; Boss, E.S.; Sathyendranath, S.; Jones, B.H.; Hoteit, I. Regional Ocean−Colour Chlorophyll Algorithms for the Red Sea. *Remote Sens. Environ.* **2015**, *165*, 64–85. [CrossRef]
15. Hirata, T.; Hardman−Mountford, N.J.; Brewin, R.J.W.; Aiken, J.; Barlow, R.; Suzuki, K.; Isada, T.; Howell, E.; Hashioka, T.; Noguchi−Aita, M.; et al. Synoptic Relationships between Surface Chlorophyll−a and Diagnostic Pigments Specific to Phytoplankton Functional Types. *Biogeosciences* **2011**, *8*, 311–327. [CrossRef]
16. Uitz, J.; Claustre, H.; Morel, A.; Hooker, S.B. Vertical Distribution of Phytoplankton Communities in Open Ocean: An Assessment Based on Surface Chlorophyll. *J. Geophys. Res. Ocean* **2006**, *111*. [CrossRef]
17. Vidussi, F.; Claustre, H.; Manca, B.B.; Luchetta, A.; Marty, J.C. Phytoplankton Pigment Distribution in Relation to Upper Thermocline Circulation in the Eastern Mediterranean Sea during Winter. *J. Geophys. Res. Ocean* **2001**, *106*, 19939–19956. [CrossRef]
18. Miranda, J.; Lotliker, A.A.; Baliarsingh, S.K.; Jena, A.K.; Samanta, A.; Sahu, K.C.; Kumar, T.S. Satellite Estimates of the Long−Term Trend in Phytoplankton Size Classes in the Coastal Waters of North−Western Bay of Bengal. *Oceanologia* **2021**, *63*, 40–50. [CrossRef]
19. Nair, A.; Sathyendranath, S.; Platt, T.; Morales, J.; Stuart, V.; Forget, M.H.; Devred, E.; Bouman, H. Remote Sensing of Phytoplankton Functional Types. *Remote Sens. Environ.* **2008**, *112*, 3366–3375. [CrossRef]
20. Devred, E.; Sathyendranath, S.; Stuart, V.; Maass, H.; Ulloa, O.; Platt, T. A Two−Component Model of Phytoplankton Absorption in the Open Ocean: Theory and Applications. *J. Geophys. Res. Ocean* **2006**, *111*, 1–11. [CrossRef]
21. Corredor−Acosta, A.; Morales, C.E.; Brewin, R.J.W.; Auger, P.A.; Pizarro, O.; Hormazabal, S.; Anabalón, V. Phytoplankton Size Structure in Association with Mesoscale Eddies off Central−Southern Chile: The Satellite Application of a Phytoplankton Size−Class Model. *Remote Sens.* **2018**, *10*, 834. [CrossRef]
22. Mouw, C.B.; Hardman−Mountford, N.J.; Alvain, S.; Bracher, A.; Brewin, R.J.W.; Bricaud, A.; Ciotti, A.M.; Devred, E.; Fujiwara, A.; Hirata, T.; et al. A Consumer's Guide to Satellite Remote Sensing of Multiple Phytoplankton Groups in the Global Ocean. *Front. Mar. Sci.* **2017**, *4*, 41. [CrossRef]

23. Blondeau−Patissier, D.; Gower, J.F.R.; Dekker, A.G.; Phinn, S.R.; Brando, V.E. A Review of Ocean Color Remote Sensing Methods and Statistical Techniques for the Detection, Mapping and Analysis of Phytoplankton Blooms in Coastal and Open Oceans. *Prog. Oceanogr.* **2014**, *123*, 123–144. [CrossRef]
24. Mouw, C.B.; Ciochetto, A.B.; Yoder, J.A. A Satellite Assessment of Environmental Controls of Phytoplankton Community Size Structure. *Glob. Biogeochem. Cycles* **2019**, *33*, 540–558. [CrossRef]
25. Gittings, J.A.; Brewin, R.J.W.; Raitsos, D.E.; Kheireddine, M.; Ouhssain, M.; Jones, B.H.; Hoteit, I. Remotely Sensing Phytoplankton Size Structure in the Red Sea. *Remote Sens. Environ.* **2019**, *234*, 111387. [CrossRef]
26. Shunmugapandi, R.; Inamdar, A.B.; Gedam, S.K. Long−Time−Scale Investigation of Phytoplankton Communities Based on Their Size in the Arabian Sea. *Int. J. Remote Sens.* **2020**, *41*, 5992–6009. [CrossRef]
27. Sahay, A.; Ali, S.M.; Gupta, A.; Goes, J.I. Ocean Color Satellite Determinations of Phytoplankton Size Class in the Arabian Sea during the Winter Monsoon. *Remote Sens. Environ.* **2017**, *198*, 286–296. [CrossRef]
28. Brewin, R.J.W.; Hirata, T.; Hardman−Mountford, N.J.; Lavender, S.J.; Sathyendranath, S.; Barlow, R. The Influence of the Indian Ocean Dipole on Interannual Variations in Phytoplankton Size Structure as Revealed by Earth Observation. *Deep−Sea Res. Part II Top. Stud. Oceanogr.* **2012**, *77–80*, 117–127. [CrossRef]
29. Iriarte, J.L.; González, H.E. Phytoplankton Size Structure during and after the 1997/98 El Niño in a Coastal up Welling Area of the Northern Humboldt Current System. *Mar. Ecol. Prog. Ser.* **2004**, *269*, 83–90. [CrossRef]
30. Racault, M.F.; Sathyendranath, S.; Brewin, R.J.W.; Raitsos, D.E.; Jackson, T.; Platt, T. Impact of El Niño Variability on Oceanic Phytoplankton. *Front. Mar. Sci.* **2017**, *4*, 133. [CrossRef]
31. Shi, W.; Wang, M. A Biological Indian Ocean Dipole Event in 2019. *Sci. Rep.* **2021**, *11*, 2452. [CrossRef]
32. Thushara, V.; Vinayachandran, P.N. Unprecedented Surface Chlorophyll Blooms in the Southeastern Arabian Sea During an Extreme Negative Indian Ocean Dipole. *Geophys. Res. Lett.* **2020**, *47*, e2019GL085026. [CrossRef]
33. Vinayachandran, P.N.; Francis, P.A.; Rao, S.A. Indian Ocean Dipole: Processes and Impacts. *Curr. Trends Sci.* **2009**, *46*, 569–589.
34. Barimalala, R.; Bracco, A.; Kucharski, F.; McCreary, J.P.; Crise, A. Arabian Sea Ecosystem Responses to the South Tropical Atlantic Teleconnection. *J. Mar. Syst.* **2013**, *117–118*, 14–30. [CrossRef]
35. Sattar, A.M.; Cheung, K.K.W. Comparison between the Active Tropical Cyclone Seasons over the Arabian Sea and Bay of Bengal. *Int. J. Climatol.* **2019**, *39*, 5486–5502. [CrossRef]
36. Saji, N.H.; Goswami, B.N.; Vinayachandran, P.N.; Yamagata, T. A Dipole Mode in the Tropical Indian Ocean. *Nature* **1999**, *401*, 360–363. [CrossRef]
37. Sayantani, O.; Gnanaseelan, C.; Chowdary, J.S. The Role of Arabian Sea in the Evolution of Indian Ocean Dipole. *Int. J. Climatol.* **2014**, *34*, 1845–1859. [CrossRef]
38. Sharma, P. Spatio−Temporal Dynamics of Phytoplankton Biomass from Ocean Color Remote Sensing and Ensemble Climate Model Simulations. Ph.D. Thesis, University of Pennsylvania, Philadelphia, PA, USA, 2016.
39. Banse, K. Seasonality of Phytoplankton Chlorophyll in the Central and Northern Arabian Sea. *Deep Sea Res. Part A Oceanogr. Res. Pap.* **1987**, *34*, 713–723. [CrossRef]
40. Madhupratap, M.; Prasanna Kumar, S.; Bhattathiri, P.M.A.; Dileep Kumar, M.; Raghukumar, S.; Nair, K.K.C.; Ramaiah, N. Mechanism of the Biological Response to Winter Cooling in the Northeastern Arabian Sea. *Nature* **1996**, *384*, 549–552. [CrossRef]
41. Kurian, S.; Chndrasekhararao, A.V.; Vidya, P.J.; Shenoy, D.M.; Gauns, M.; Uskaikar, H.; Aparna, S.G. Role of Oceanic Fronts in Enhancing Phytoplankton Biomass in the Eastern Arabian Sea during an Oligotrophic Period. *Mar. Environ. Res.* **2020**, *160*, 105023. [CrossRef]
42. Prasanna Kumar, S.; Nuncio, M.; Narvekar, J.; Ramaiah, N.; Sardesai, S.; Gauns, M.; Fernandes, V.; Paul, J.T.; Jyothibabu, R.; Jayaraj, K.A. Seasonal Cycle of Physical Forcing and Biological Response in the Bay of Bengal. *Indian J. Mar. Sci.* **2010**, *39*, 388–405.
43. Prasanna Kumar, S.; Roshin, R.P.; Narvekar, J.; Dinesh Kumar, P.K.; Vivekanandan, E. What Drives the Increased Phytoplankton Biomass in the Arabian Sea? *Curr. Sci.* **2010**, *99*, 101–106.
44. Shi, W.; Wang, M. Phytoplankton Biomass Dynamics in the Arabian Sea from VIIRS Observations. *J. Mar. Syst.* **2022**, *227*, 103670. [CrossRef]
45. Currie, J.C.; Lengaigne, M.; Vialard, J.; Kaplan, D.M.; Aumont, O.; Naqvi, S.W.A.; Maury, O. Indian Ocean Dipole and El Niño/Southern Oscillation Impacts on Regional Chlorophyll Anomalies in the Indian Ocean. *Biogeosciences* **2013**, *10*, 6677–6698. [CrossRef]
46. Beckers, J.M.; Rixen, M. EOF Calculations and Data Filling from Incomplete Oceanographic Datasets. *J. Atmos. Ocean. Technol.* **2003**, *20*, 1839–1856. [CrossRef]
47. Jayaram, C.; Priyadarshi, N.; Pavan Kumar, J.; Udaya Bhaskar, T.V.S.; Raju, D.; Kochuparampil, A.J. Analysis of Gap−Free Chlorophyll−a Data from MODIS in Arabian Sea, Reconstructed Using DINEOF. *Int. J. Remote Sens.* **2018**, *39*, 7506–7522. [CrossRef]
48. Brewin, R.J.W. Detecting Phytoplankton Size Class Using Satellite Earth Observation September 2010. 2011, p. 276. Available online: https://pearl.plymouth.ac.uk/handle/10026.1/317 (accessed on 10 June 2022).